High-Frequency Metal-Oxide Varistor Modeling Response to Early-time Electromagnetic Pulses

Tyler Bowman, Matt Halligan, and Rodrigo Llanes

Sandia National Laboratories

Albuquerque, NM

tbowma@sandia.gov, mhallig@sandia.gov, and rllanes@sandia.gov

Abstract—The electric power grid is one of the most critical infrastructures in the modern world, and the continued protection and resilience of this system from threats is of significant concern. One such set of threats is nanosecond-scale transient effects generated by high-altitude electromagnetic pulses, for which the effect on the power grid is still being studied. Lightning surge arresters serve as the current grid protection against fast transients but are designed and modeled for protection against lightning and switching transients. Surge arrester response to faster transients is not well known. This work defines a scalable metal-oxide surge arrester model with specific consideration to frequencies attributed to fast transient overvoltages from electromagnetic pulses. Measurements using vector network analyzer sweeps at low and high bias as well as high-voltage I-V curve traces are presented to define arrester behavior and to parameterize it from measurement data. The proposed model is compared to the standard IEEE model for lightning arresters in this paper. Furthermore, model parameters are defined by scalable terms to be easily implemented for transmission-level devices. The scalable model enables enhanced assessment of protection levels and grid susceptibility against fast transients.

Index Terms—Arresters, Electromagnetic transients, Electromagnetic pulse (EMP), Power system protection, Power system transients, Surge protection

I. INTRODUCTION

The electric power grid is a complex system that supports modern society. This system is critical to many operations due to the increasing reliance on electricity. There is increasing interest to improve electric grid resiliency to both natural and man-made electromagnetic insults. Some insults under consideration for protection include lightning, geomagnetic disturbances, intentional electromagnetic interference, and electromagnetic pulses (EMPs).

The focus of this paper is on modeling metal-oxide varistor (MOV) response to a high-altitude EMP (HEMP) event due to the prevalence of MOVs throughout the electric grid. HEMP events generate significant electromagnetic fields on the earth's surface, which couple to overhead powerlines and deliver a conducted impulse to components in the power grid. Lightning surge arresters (LSAs) are the primary defense mechanism against fast transient pulses for power transformers in transmission-level substations. Many modern surge arresters are gapless, and typically comprise of a MOV material such as ZnO and other additive materials. These surge arresters are routinely tested with microsecond-scale rise time pulses, which are common for lightning and switching events. LSAs are therefore anticipated to function normally for mid-time HEMP (E2), and late-time HEMP (E3) is not expected to generate enough voltage to be relevant for overvoltage protection. In contrast, early-time HEMP, referred to as E1, has conducted pulse risetimes of 10's of nanoseconds [1]. The behavior of LSAs in response to E1 overvoltages is largely unknown, and there is a need to investigate LSA response at the nanosecond timescale.

Conducted environments generated from radiated E1 environments at substations vary significantly due to line orientation, line height, geographical location with respect to the E1 origin, and several other factors. LSA response evaluation to conducted E1 environments requires a surge arrester model that captures component dynamics at nanosecond timescales. Several authors developed circuit models for MOV arresters to simulate lightning protection. One of the earliest models and present standards was published by IEEE [2], while subsequent models have focused on using parameters based on electrical properties only [3], simplified estimations of nonlinear varistor behavior [4], or wideband response accuracy [5]. These models were formulated to describe arrester behavior for lighting-like impulses (microsecond timescales) with spectral content up to a few hundred kHz. Meanwhile, standard E1 field definitions have spectral content up to 100 MHz [6]. Nanosecond-scale pulse simulations of existing arrester models show widely varying responses compared to consistent lightning response predictions as shown later. Thus, there is a need to develop a fast transient, high frequency surge arrester model that can be used to predict the E1 surge arrester response, to identify any design limitations of existing arresters, and to assess what protection, if any, is provided by LSAs in response to HEMP events.

This work defines a scalable model for MOV surge arresters based on small-scale ZnO devices. Experimental results are

presented from high frequency sweeps and bias-dependent property measurements to parameterize the model. The model can be scaled for distribution and transmission level arresters, and the latter is demonstrated here for applicability to system-level grid simulations.

II. MATERIALS AND BASE MODEL

A. Physical Arrester Model

The arrester model used in this work is based on the physical configuration of the MOV material in an assembled LSA. Example arrester assembly cutouts are shown in Fig. 1 for an 18 kV, 6 kV, and 3 kV arrester. A stack of ZnO discs are used as the MOV material in the arrester, where metal spacers on the ends and between ZnO discs are used to achieve the desired device length. A completed assembly is wrapped in fiberglass and a polymer housing with metal contacts protruding on each end.

Polymer Casing with   Bulk ZnO
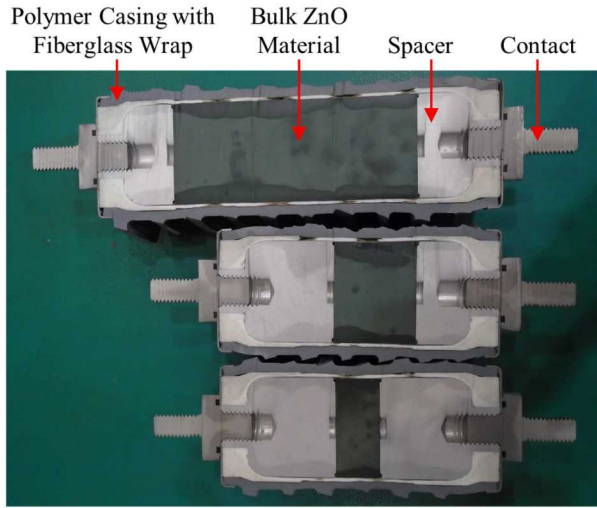Fiberglass Wrap   Material   Spacer   Contact

Figure 1. Fully assembled metal-oxide LSAs with 18 kV (ZIP0018), 6 kV (ZIP0006), and 3 kV (ZIP0003) rated voltages (pictured top to bottom).

A physical circuit model representing the assemblies in Fig. 1 is shown in Fig. 2. The ZnO stack is represented as a capacitance, C, with a parallel, non-linear, bias-dependent resistance, R_{Bias}, representing the varistor behavior. The series inductance, L, corresponds to the inductance created from the full length of the arrester, which is significant for fast transients such as E1. This model applies to many arrester assemblies ranging from single puck arresters to transmission-scale assemblies and will be referred to for the remainder of this paper.

The primary frequency-dependent behavior of an arrester under low biasing conditions is controlled by the L and C elements shown in Fig. 2. R_{Bias} defines the principal non-linear operation of the MOV resistance and is divided into three operational regions [5]. The first region, the leakage region, has little current conduction (< 10 μA observed) and has an approximately fixed resistance. The second region, the breakdown or transient overvoltage (TOV) region, encompasses currents from the μA range to approximately 1 kA and has resistance decreasing along a power curve to maintain voltage near a geometry-dependent clamping level. The third region, the up-turn region, is defined for currents above 1 kA, where the rate of
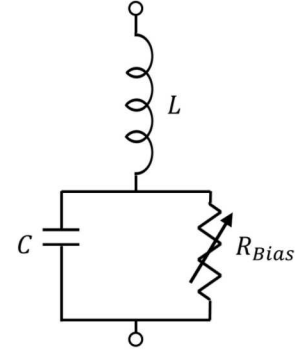

Figure 2. Physical surge arrester circuit diagram and proposed model.

decrease in resistance is reduced as the grain resistance of the sintered ZnO material begins to dominate the response [7]. Most modern arresters have the same fundamental geometry consisting of a column of MOV pucks with metal spacers and contacts to obtain the desired length. Therefore, physically defined model parameters obtained for smaller MOV arresters are directly scalable to larger transmission arresters with some consideration for column dimensions.

Measurements were performed on individual MOV puck arresters and small, fully assembled distribution arresters to generate the scalable arrester model. Five different puck arrester sizes were obtained from Dean Technologies [8] as shown in Fig. 3 with sizes and ratings listed in Table I. The fully assembled arresters used in this study were MacLean Power Systems ZIP0003, ZRP0003, ZIP0006, and ZIP0018 models rated at 3 kV, 3 kV, 6 kV, and 18 kV, respectively [9].
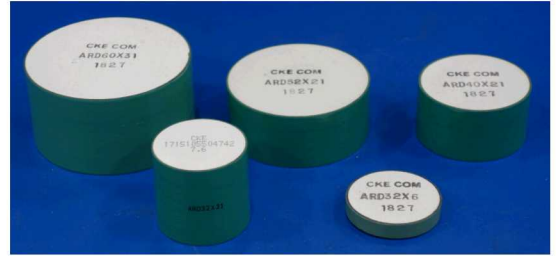

Figure 3. Dean Technologies metal-oxide varistor pucks used for small-scale measurements.

TABLE I.   MOV PUCK DIMENSIONS AND VOLTAGE RATINGS

Name	Dimensions	Rating
ARD32X6	32 mm (D) × 6 mm (H)	0.5 kV
ARD32X31	32 mm (D) × 31 mm (H)	4.5 kV
ARD40X21	40 mm (D) × 21 mm (H)	3.0 kV
ARD52X21	52 mm (D) × 21 mm (H)	3.0 kV
ARD60X31	60 mm (D) × 31 mm (H)	4.5 kV

B. Measurement Setups

Three test setups were used to quantify the circuit component values in Fig. 2 for various LSAs. First, low voltage vector network analyzer (VNA) measurements were performed using a frame to mount the devices over a ground plane for high frequency analysis. Sweeps were performed across the available VNA range from 9 kHz to 4.5 GHz. Frequency-domain measurements showed a broadband capacitive behavior and self-resonance at high frequency from the arrester inductance, which

are used to define the LC elements of the model experimentally. Next, an I-V curve tracer as described in [10] was used to quantify non-linear current and voltage characteristics represented by R_{Bias}. The I-V curve tracer used millisecond-scale, short duty cycle pulses to measure bias-dependent resistance in the leakage and early breakdown regions of the arresters. The testbed output was limited to 18 kV or 20 mA in all measurements. Additional resistance values for model development were obtained from manufacturer data [8], [9] to produce a broad definition of the non-linear resistance. The last setup for model quantification was a high-voltage bias tee testbed. This testbed enabled a high-voltage DC bias across the arresters under test while small-signal VNA measurements were performed as shown by the schematic in Fig. 4. Additional details on the measurement setups are provided in the following sections.
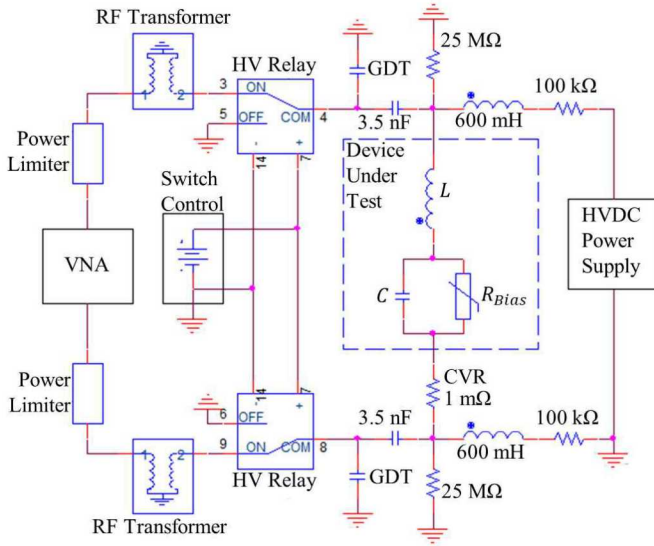

Figure 4. High voltage bias tee circuit used for high bias VNA measurements on MOVs.

III. MEASUREMENTS AND MODEL PARAMETERIZATION

A. Low Voltage Bias VNA Measurements

Results from low voltage bias VNA sweeps of the MOV pucks and full arresters all followed a similar trend. Example results from the ZIP0018 arrester are shown in Fig. 5, where the arrester impedance was extracted from the parameter B in the $ABCD$ matrix calculated from measured S-parameters. Results are shown up to 100 MHz based on the anticipated spectral content of a radiated E1 pulse [6] and because the experimental setup reaches a length of $\lambda/20$ around 150 MHz, beyond which the setup is no longer electrically small. The primary behavior of the LSA for the continuous wave sweeps is capacitive up to the resonance near 30 MHz and inductive above resonance. Low frequency noise caused oscillations above 90° in the measured phase of the transfer parameter S_{21}, resulting in the rapid phase shifts observed below 100 kHz in the calculated arrester impedance.

Low voltage bias VNA measurements were performed across all the MOV pucks listed in Table I. The effective relative permittivity was calculated from puck geometry and the extracted capacitance information for each VNA measurement.

The average effective relative permittivity was 755 and is slightly lower than values found in literature for ZnO material [11]. A correlation exists between the radius, length, and 10 kA residual voltage for an arbitrary ZnO disk [12]. Therefore, it is possible to estimate the dimensions of the internal MOV with respect to arrester discharge class and the residual voltage peak for a 10 kA test signal. This avoids inaccuracies that might arise from using external arrester dimensions without knowledge of the size or number of metal spacers in the overall assembly. The approximations of the relative permittivity and MOV dimensions within the assembly are used to calculate the capacitance in the scalable model for transmission-level arresters.

Also plotted in Fig. 5 is the impedance from the circuit model in Fig. 2 and the IEEE model in [2]. For the proposed model, the resistance R_{Bias} is large for the low voltage bias VNA sweep, so the measured impedance is entirely defined by C and L. These values are calculated from the measured broadband capacitive behavior and from the first resonance, respectively. The proposed model impedance curve is within 0.25 dB of the measurement data up to the resonance frequency. In contrast, the IEEE model is defined by the arrester length and 10 kA residual discharge following the process in [2]. The IEEE model shows a minimum 10 dB magnitude difference from measurements in the 1-10 MHz range where both curves are capacitive. This magnitude difference increases to 15 dB in the inductive region for the IEEE model. Thus, while the IEEE model is focused on accurate response to lightning-like test waveforms, it does not capture arrester reactive elements well, namely the inductance, that affects faster transient responses.

Example transient responses of the proposed model of Fig. 2 and the IEEE arrester model are shown in Fig. 6. Here, SPICE models of the 18 kV arrester using the proposed circuit and the IEEE circuit are simulated for response to a lightning-like 8/20 10 kA current waveform (Fig. 6a) and an E1-like voltage waveform obtained from coupling calculations for a 5 km line in [1] using the IEC 61000-2-9 E1 waveform in [6] (Fig. 6b). In Fig. 6a, the primary response by the arrester in both models is from the changing varistor resistance for the slower lightning waveform. However, in Fig. 6b for the E1-like waveform, the IEEE
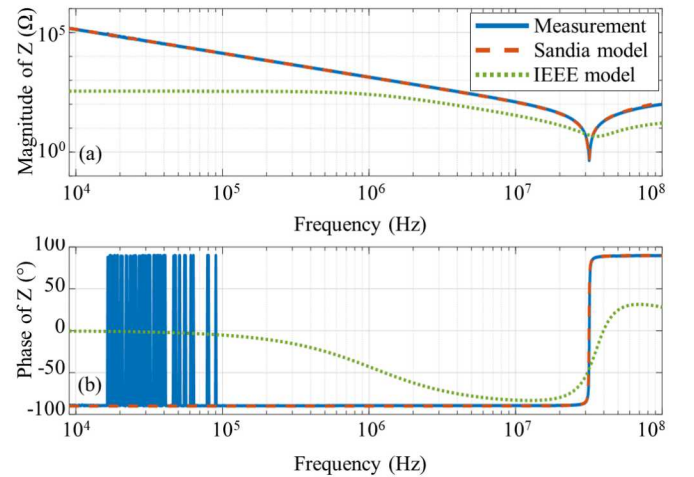

Figure 5. (a) Calculated impedance magnitude and (b) impedance phase of the 18 kV ZIP0018 arrester obtained via a low voltage VNA sweep. The impedance of the proposed model and the IEEE arrester model are also shown for comparison.

model significantly underpredicts the initial voltage peak compared to the proposed model, which is attributable to differences in modeling the arrester inductance. Accurate modeling of the inductance is critical for predicting the response time of the assembled arrester, as the ZnO varistor behavior is expected to operate on sub-nanosecond scales when electrical length is negligible [13].
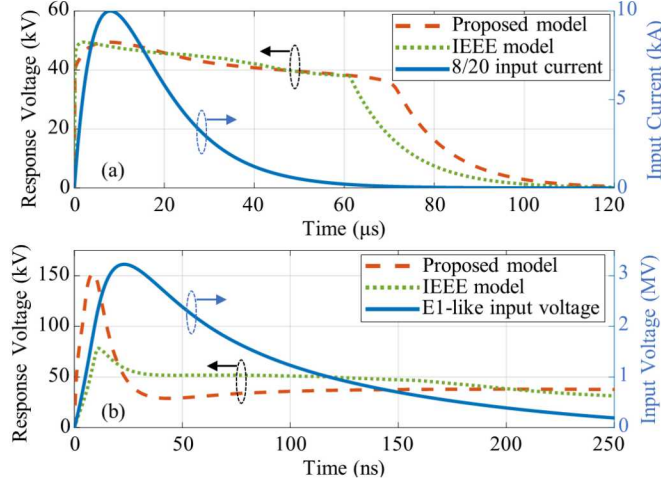

Figure 6. Simulated voltage responses of the proposed model and IEEE arrester model for (a) an 8/20 10 kA current waveform and (b) an E1-like voltage waveform.

B. I-V Curve Tracing

I-V curve tracing was performed to quantify resistance values in the leakage and early breakdown regions of MOV performance. An example of these results is shown in Fig. 7 for the Maclean Power Systems ZRP0003 arrester assembly shown in Fig. 7a. The results in Fig. 7b illustrate the anticipated varistor behavior, where the arrester resistance is relatively stable (around 5 GΩ) at the lower range of applied voltage. There is some noise in the data due to the microamp-scale leakage current being measured through the arrester. Once the bias reaches the clamping voltage, the resistance begins to decrease exponentially and the current significantly increases. This I-V curve is then combined with manufacturer data for switching surges and 8/20 test pulses [9] to extend the varistor behavior further into the breakdown and up-turn regions. The low current measurement data and high current manufacturer data are combined into the varistor response up to 40 kA in Fig. 8, alongside the simulated I-V curves of the proposed model and IEEE model. The IEEE model defines the varistor behavior using a current-voltage lookup table from 100 A to 20 kA or is alternately defined using diode-like power function curves. The first option is shown in Fig. 8, where the resistance I-V curve is undefined below 100 A and here is set to scale linearly to the origin with a constant resistance. The power curve option similarly ignores much of the breakdown/TOV region, and in both implementations of the IEEE model the up-turn region is treated as a purely inductive effect. In the proposed model the I-V curve is instead based on (1), which uses a four parameter logistic (4PL) regression curve to fit the low current data and adds a second exponential term to define the non-linear up-turn region.
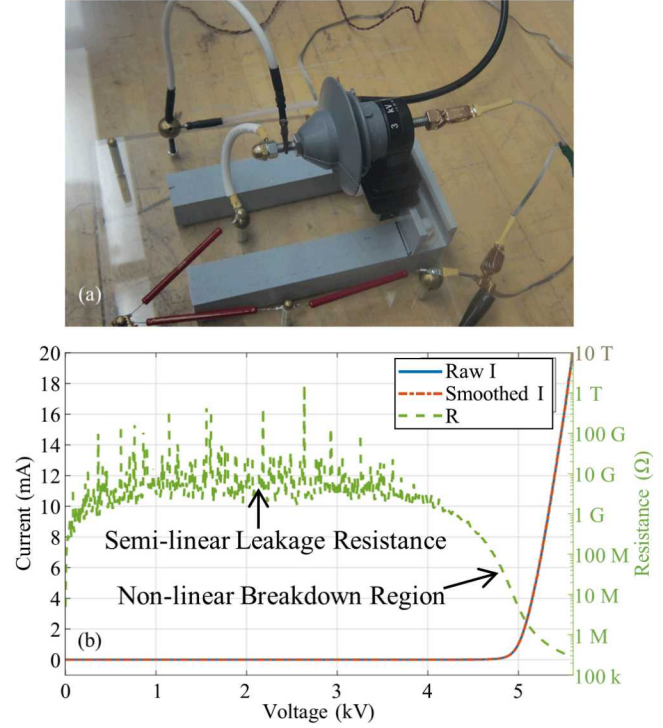

Figure 7. (a) 3 kV ZRP0003 arrester mounting configuration with the I-V curve tracer. (b) Measured I-V characteristics and calculated resistance with high voltage bias.

$$I = V \left/ \left(\frac{a}{1+\left(\frac{V}{c}\right)^b} + \frac{d}{\left(\frac{V}{f}\right)^e} \right) \right. \tag{1a}$$

$$a = R_{Bias,LV} \qquad\qquad d = V_{10}/I_{10}$$
$$b = \frac{log(a/R_{switch})}{log(V_{switch}/c)} \qquad e = \frac{log(d/R_{V_{max}})}{log(V_{max}/f)} \tag{1b}$$
$$c = V_{clamp} \approx \sqrt{2}V_{rated} \qquad f = V_{10}$$

I and V in (1a) are the current through and voltage across the varistor element R_{Bias} in Fig. 2. For the parameters in (1b), $R_{Bias,LV}$ is the leakage resistance at low bias, V_{switch} and R_{switch} are the reported switching surge voltage from the arrester manufacturer and equivalent resistance, V_{clamp} is the measured clamping voltage, V_{rated} is the arrester voltage rating, V_{10} is the residual voltage peak reported for a 10 kA (I_{10}) test pulse, and V_{max} and $R_{V_{max}}$ are the residual voltage peak and equivalent resistance for the highest reported 8/20 test pulse (usually 40 kA).

Parameters d-f require only manufacturer data, while parameters a-c use measurement data when available or are approximated based on manufacturer data. As with the capacitance measurements, the leakage resistance $R_{Bias,LV}$ is calculated from the estimated MOV dimensions and a previously measured effective resistivity. This allows a definition of a in (1b) without the need to measure the leakage resistance, though the resistivity of ZnO at low bias varies significantly with an effective resistivity of 10^6-10^9 Ω-m across measurements and in literature [14]. The specific resistivity of the ZnO does not show
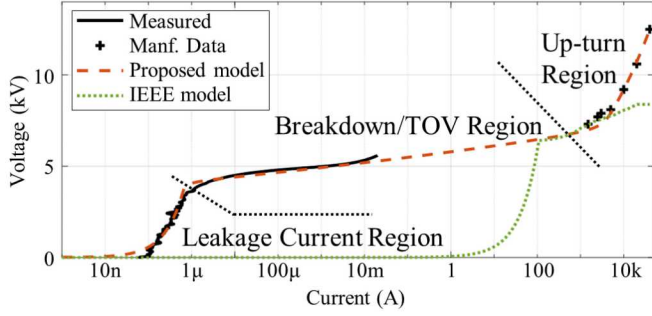
Figure 8. Measured and modeled I-V curve for a 3 kV ZRP0003 arrester.

a significant impact on simulated pulse response of the arrester for E1-like signals, which typically generate hundreds to thousands of amps through the arrester and is dependent primarily on the resistance in the breakdown region.

Equation (1) is easily integrated into SPICE-based applications as a voltage-dependent current source without the need for a voltage table lookup often used by IEEE and other models, and (1) is more flexible at defining multiple I-V curve regions than diode or power curve models. The primary benefits of this implementation are two-fold. First, the equation-based model results in a simpler circuit structure in the simulation netlist and naturally crosses the origin without the need for additional table manipulation or opposite-facing elements in the circuit design. Second, the equation-based method provides a realistic upper limit to the arrester impedance by modeling the leakage resistance, which is important for simulations where the arrester may be in parallel with other large impedances such as a power transformer.

C. High Voltage Bias VNA Sweeps

High voltage (HV) bias tee measurements were performed on MOV pucks to quantify capacitance variation with respect to an applied DC bias. The circuit for the high voltage bias tee setup is shown in Fig. 4. The MOV pucks were placed under a high voltage DC bias up to 16 mA or 22 kV from the DC branch (right hand side in Fig. 4). Then, the AC branch (left hand side in Fig. 4) was switched into the circuit to acquire the puck VNA sweep under a DC bias. Capacitors on the AC path and inductors on the DC path provided isolation between the two branches so that only the device under test was exposed to both signals, and additional gas discharge tubes, RF transformers, and power limiters provided protection to the VNA from high voltage leakage. High voltage probes on both sides of the MOV puck measured the bias voltage while a current-viewing resistor was probed for current. Each device in the AC branch of the circuit was measured individually to de-embed puck characteristics from the overall VNA measurement using block analysis. The analysis of the VNA sweeps at each DC bias point was the same method performed for the low voltage sweep in Fig. 5, and the calculated parameters were checked for trends in relation to the bias across the puck after accounting for other resistive losses in the setup.

The calculated puck capacitance as a function of DC bias is shown in Fig. 9 for 1 kV steps of the HVDC power supply. The absolute capacitance is shown in Fig. 9a, and a normalized capacitance with respect to low biasing conditions is shown in
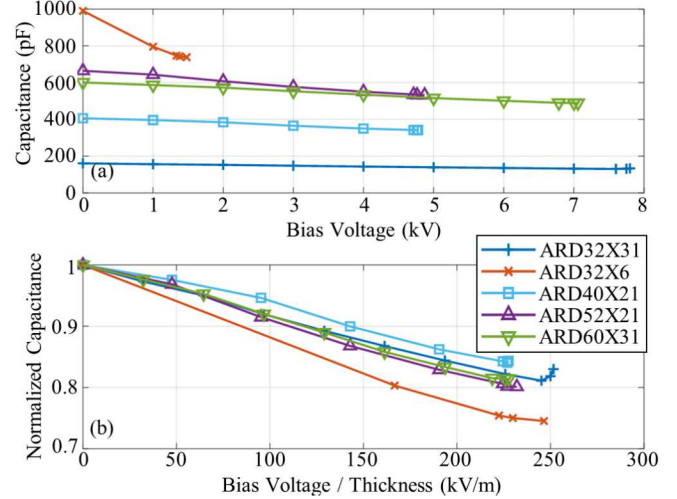

Figure 9. Bias-dependent capacitance of the Dean Technologies MOV pucks calculated from high voltage bias tee measurements. (a) Calculated capacitance versus bias voltage and (b) normalized capacitance versus bias voltage scaled by puck thickness.

Fig. 9b. The bias voltage is normalized by puck thickness in Fig. 9b to illustrate the normalized MOV capacitance as a function of internal electric field. The clustering of points at the high bias end of the plots corresponds to the clamping at high bias, which prevented the voltage across the puck from increasing even as the power supply was increased.

The functional response of the measured MOV capacitance was expected to take the form of a "U" shape as observed in [15]. Only the initial decreasing capacitance trend was captured with increasing bias voltage in most measurements due to test setup limitations. The capacitance is further defined by the normalized results in Fig. 9b, which show a decrease in the capacitance with respect to bias voltage when accounting for the thickness of the individual pucks. The ARD32X31 measurement near 250 kV/m was the only data set to capture a small increase in capacitance at high bias. The residual voltage across the pucks for a typical 10 kA signal would not push the capacitance below 70% of the original value based on the Fig. 9 capacitance measurements. Simulations have shown that this degree of shift in capacitance has negligible effects on the arrester model response to fast transients and therefore does not need to be implemented into the circuit in Fig. 2.

D. Scaling Example for a Transmission-Level Arrester

Measurement and modeling results are shown for small-scale arresters in the previous sections. The utility of these small-scale arrester results for large, gapless arresters with the same ZnO materials is presented through an example. The modeling process will be demonstrated for a MacLean Power Systems ZIP0108 arrester rated at 108 kV. Characteristics of the 108 kV arrester from the manufacturer are given in Table II [9].

TABLE II.   ZIP0108 ARRESTER MANUFACTURER DATA

Arrester Height	Discharge Class	V_{Switch} (@ 500 A)	V_{10} (@ 10 kA)	V_{Max} (@ 40 kA)
1.218 m	2	222.92 kV	279.81 kV	339.69 kV

5

The arrester inductance as shown in Fig. 2 is estimated with a typical value of 1 nH/mm total length [5]. Thus, the 108 kV arrester has an estimated 1.218 µH inductance. The arrester capacitance as depicted in Fig. 2 is estimated from approximate dimensions of the MOV column and average measured effective permittivity. The diameter of the enclosed MOV column is estimated to scale linearly based on arrester class from 32 mm (class 1) to 100 mm (class 5) [12]. The column length is estimated from the column radius and V_{10} based on nominal discharge values reported in [12]. A power fit curve provides the following estimation in (3).

$$l_{ZnO} = \frac{V_{10}(r_{ZnO})^{0.2844}}{1.3 \times 10^5} \text{ (H)} \qquad (3)$$

l_{ZnO} is the calculated MOV column length, r_{ZnO} is the estimated column radius, V_{10} is the reported 10 kA discharge voltage from the manufacturer, and H is the arrester height. The arrester capacitance is calculated as 16.4 pF with the estimated diameter and length of the MOV column and an average measured effective relative permittivity of $\varepsilon_r = 755$.

R_{Bias} as shown in Fig. 2 is estimated from (1). The leakage resistance a is estimated using the same MOV column dimensions with $\rho_{eff} = 10^8$ Ω-m. Clamping voltage c is estimated from the rated voltage of 108 kV, and b, d, e, and f are calculated using the values in Table II. The resulting parameter values are reported in Table III and are incorporated into the arrester model by using a voltage-dependent current source and (1) to define the varistor behavior.

TABLE III.   ZIP0108 SCALED RESISTANCE PARAMETERS

a	b	c	d	e	f
39.70 GΩ	48.407	152.73 kV	27.98 Ω	6.149	279.81 kV

IV.   CONCLUSION

In this paper a scalable model for MOV surge arresters is proposed for the specific application of modeling responses to nanosecond-scale transients. Experimental data from MOV pucks and distribution arresters shows the high frequency response of arresters is readily mapped to LC elements in a circuit. Likewise, an equation based on manufacturer data and minimal approximations provides a fit for the bias-dependent resistance that defines the non-linear MOV operation. The model is scalable to larger devices by accounting for the change in the MOV dimensions with respect to arrester class and voltage ratings. It is noted that while high voltage pulse testing provides the most direct indication of arrester transient response, models generated from these limited data sets are not readily scalable for other arrester sizes and do not predict the response for differing pulses. These limitations of a pulse-response-only approach are not present in the proposed model and is an advantage of the model.

Though not necessary for model generation, pulse testing will still provide key validation of the proposed model for accuracy of the time domain response. This is being investigated for follow-up testing of the MOV materials using a pulser operating on the nanosecond scale similar to conducted E1 environment proposed in [16].

REFERENCES

[1] S. Campione, L. K. Warne, M. Halligan, O. Lavrova, and L. San Martin, "Decay Length Estimation of Single-, Two-, and Three-Wire Systems Above Ground Under HEMP Excitation," *Progress In Electromagnetics Research B*, vol. 84, p. 23-42, 2019.

[2] IEEE Working Group 3.4.11, "Modeling of Metal Oxide Surge Arresters," *IEEE Trans. Power Delivery*, vol. 7, no. 1, pp. 302-309, Jan. 1992.

[3] P. Pinceti and M. Giannettoni, "A simplified model for zinc oxide surge arresters," *IEEE Trans. Power Delivery*, vol. 14, no. 2, pp. 393-398, Apr. 1999.

[4] F. Fernández and R. Díaz, "Metal-oxide surge arrester model for fast transient simulations," The Internation Conference on Power System Transients IPAT, 2001.

[5] V.S. Brito, G.R.S. Lira, E.G. Costa, and M.J.A. Maia, "A Wide-Range Model for Metal-Oxide Surge Arrester," *IEEE Trans. Power Delivery*, vol. 33, no. 1, Feb. 2018.

[6] *Electromagnetic compatibility (EMC) - Part 2: Environment - Section 9: Description of HEMP environment - Radiated disturbance.* IEC 61000-2-9:1996, 1996.

[7] T.K. Gupta, "Application of zinc oxide varistors," *J. Amer. Ceram. Soc.*, vol. 73, no. 7, pp. 1817-1840, July 1990.

[8] ARD Series – CKE Metal Oxide Varistors | Dean Technologies, [https://www.deantechnology.com/catalog/cke/metal-oxide-varistors/high-voltage-bare-disc-surge-arrestors/ard].

[9] MacLean Power Systems – Arresters, [https://www.macleanpower.com/products/index.asp?DEPARTMENT_ID=2854].

[10] L. J. Rashkin *et al.*, "Miniature high voltage, high temperature component package development," in *Proc. 2016 IEEE Int. Power Modulator and High Voltage Conf.*, San Francisco, CA, 2016, pp. 62-67.

[11] L.M. Levinson and H.R. Philipp, "AC properties of metal-oxide varistors," *J. Appl. Phys.*, vol. 47, no. 3, pp. 1117-1122, March 1976.

[12] V. Hinrichsen, *Metal-Oxide Surge Arresters in High-Voltage Power Systems*, 3rd ed., © Siemens AG 2011.

[13] H.R. Philipp and L.M. Levinson, "ZnO varistors for protection against nuclear electromagnetic pulse," *J. Appl. Phys.*, vol. 52, no. 2 pp. 1083-1090, February 1981.

[14] P.R. Emtage, "The physics of zinc oxide varistors," *J. Appl. Phys.*, vol. 48, no. 10, pp. 4372-4384, Oct. 1977.

[15] G.D. Mahan, L.M. Levinson, and H.R. Philipp, "Theory of conduction in ZnO varistors," *J. Appl. Phys.*, vol. 50, no. 4, pp. 2799-2812, Apr. 1979.

[16] *Electromagnetic compatibility (EMC) - Part 2-10: Environment - Description of HEMP environment - Conducted disturbance.* IEC 61000-2-10:1998, 1998.